



# Nature of V-shaped defects in HgCdTe epilayers grown by molecular beam epitaxy

I.V. Sabinina\*, A.K. Gutakovsky, Yu.G. Sidorov, A.V. Latyshev

*Institute of Semiconductor Physics, Siberian Branch of Russian Academy of Science, Pr. Ac. Lavrentyeva, 13, Novosibirsk 630090, Russia*

Received 23 June 2004; accepted 4 October 2004

Communicated by A.Y. Cho

Available online 15 December 2004

## Abstract

The microstructure and micromorphology of V-shaped defects in (301) and (112) HgCdTe layers grown by molecular beam epitaxy (MBE) have been investigated in detail on the consecutive stages of its formation by transmission and high-resolution electron microscopy (TEM and HREM) and atomic force microscopy (AFM). The nature of V-shaped defects in epilayers grown by MBE is reported. It was shown that the nucleation of a V-shaped defects occurs on the relief perturbations and its growth is stimulated by non-optimal growth conditions. The formation of V-shaped defect begins from the capture of excess Te along the growth front at the steady-state stages of HgCdTe growth and along the irregularities on the surface of the CdTe buffer layer at the initial stages. High-resolution observations established the occurrence of elemental Te and misoriented HgCdTe grains along the macrosteps on the growth HgCdTe surface. The captured Te initiates the formation of walls with disordered structure (DS walls) extended along the growth direction and containing misoriented HgCdTe grains, Te precipitates and dislocations observed by TEM. While growing, vertical columns packed with stacking faults and bounded by DS walls are formed. We find that these columns can be considered as the basic part of the V-shaped defect in HgCdTe grown by MBE. Due to the continual Te nucleation and twinning inside the defect area, polycrystalline growth can occur.

© 2004 Elsevier B.V. All rights reserved.

PACS: 61.30.Hn; 68.55.Ln; 68.37.Lp; 68.37.Ps

Keywords: A1. Defects; A3. Molecular beam epitaxy; B1. Tellurites; B2. Semiconducting II–VI materials; B3. Infrared devices

## 1. Introduction

Typical threading defects, which are called voids [1–5] or surface-craters [6–8], are commonly observed on the surfaces of HgCdTe epilayers grown by molecular beam epitaxy (MBE). The

\*Corresponding author. Tel.: +007 3832 333 283; fax: +007 3832 331 080.

E-mail address: [sabinina@isp.nsc.ru](mailto:sabinina@isp.nsc.ru) (I.V. Sabinina).

cross-sections of these defects extend to the top surface, so we called them V-shaped defects [9]. A typical density of V-shaped defects is about  $10^3 \text{ cm}^{-2}$ . When a V-shaped defect is located within the active area of a photo-diode, it leads to diode parameter deterioration [2]. Because of this, the density of V-shaped defects must be minimized, especially for the fabrication of local plane infrared detector arrays (FPAs). In spite of the importance of this problem, the mechanisms of nucleation and multiplication of the defects during MBE have not been well investigated. The important role of elemental Te in the formation of V-shaped defects was shown in our paper [9] and is suggested now in other papers [6–8]. Several groups [3,5] demonstrated the reduction in defect density to  $100\text{--}300 \text{ cm}^{-2}$  by the optimization of growth conditions and careful efforts in substrate preparation. For the reproducibility and improvement of this result, in our opinion, it is necessary to investigate the microstructure and mechanism of V-shaped defect formation in detail. In this paper we report the investigations of the microstructure and micromorphology of HgCdTe epilayers grown by MBE, using transmission and high-resolution electron microscopy (TEM, HREM) and atomic-force microscopy (AFM). A comparison between the TEM image of the defect microstructure with the AFM image of its micromorphology on different stages of HgCdTe growth is effective for the investigation of the V-shaped defect formation mechanism. Our studies of (301), (112), (100) HgCdTe epilayers grown on the substrates from GaAs, Si, CdTe allow one to conclude that the origin and V-shaped defect formation mechanism are independent of substrate material and orientation. The defect shape and size vary with substrate orientation and growth conditions. This paper reports on the results of investigation of the V-shaped defect formation mechanism using (301) HgCdTe and (112) HgCdTe layers.

## 2. Experiments

HgCdTe epilayers were grown by MBE on (301) and (112)B oriented substrates from

different materials: GaAs, Si, CdTe. The hetero-epitaxial structures grown on GaAs and Si substrates include a ZnTe buffer layer  $\sim 100 \text{ nm}$  thick, a CdTe buffer layer  $6\text{--}8 \mu\text{m}$  thick and a  $\text{Hg}_{0.78}\text{Cd}_{0.22}\text{Te}$  layer  $\sim 10 \mu\text{m}$  thick. MBE growth of HgCdTe heterostructures on GaAs and Si substrates has been reported in detail in papers [10] and [11], respectively. The microstructure of HgCdTe layers was studied using TEM and HREM with a JEOL-4000 EX. The micromorphology of the HgCdTe layer surface was studied using AFM (Solver P-47H, NT-MDT) with a  $47 \times 47 \mu\text{m}^2$  scan in semicontact mode at ambient conditions. The samples for TEM and HREM were prepared both in plan-view configurations parallel to the growth surface and in cross-sections by the original technique based on chemimechanical polishing [12].

## 3. Results and discussion

According to the AFM study of (301) HgCdTe layers, two types of surface morphologies are observed: the isotropic relief when valleys and ridges are randomly arranged and the anisotropic one when valleys and ridges are oriented approximately along the [010] direction (Fig. 1). It should be noted that isotropic relief is observed under optimum growth conditions, whereas anisotropic relief is observed under a deviation of growth conditions from optimum. The anisotropic relief may be defined as a system of macrosteps oriented approximately along the [010] direction. AFM observations of a considerable body of HgCdTe layers indicate that the average height ( $h$ ) of macrosteps and the distance between them ( $d$ ) depend on surface orientation and growth conditions. The AFM image shown in Fig. 1b is an example of the anisotropic periodic relief observed on the (301) HgCdTe surface with  $h \sim 5 \text{ nm}$  and  $d \sim 100 \text{ nm}$ .

AFM and TEM investigations show that V-shaped defects are complicated defects composed of twin lamellas (TLs), stacking faults (SFs) and areas with disordered structure (DS) with a high concentration of elemental Te that can run to 3% according to electron probe microanalysis

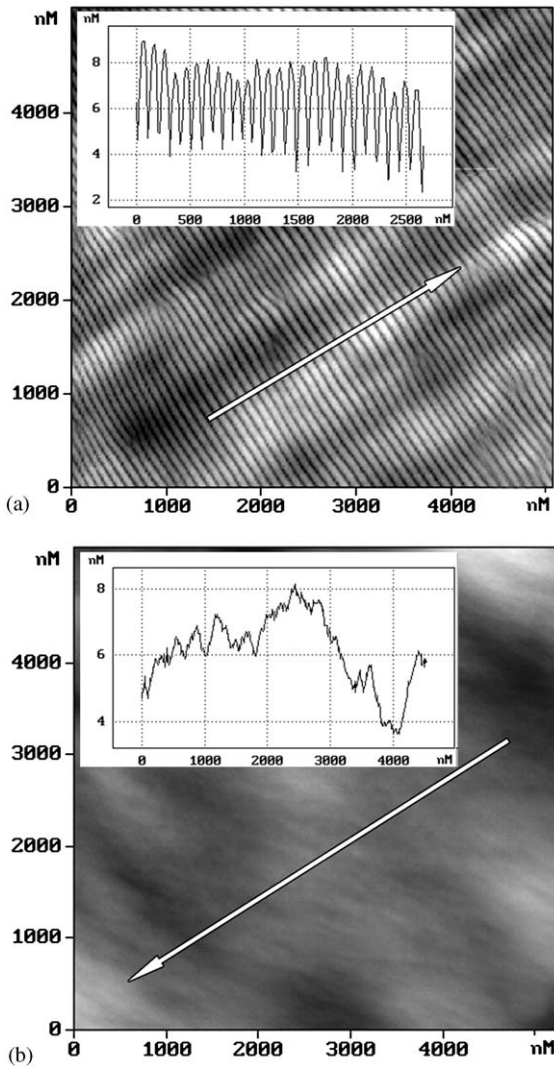


Fig. 1. AFM images of the (301) surface of HgCdTe film grown under non-optimal (a) and optimal (b) growth conditions and the corresponding height profile along white lines.

(EPMA) [10]. Near the V-shaped defects, typical surface irregularities are observed. Fig. 2 shows the typical AFM (a) and TEM (b) images of a V-shaped defect observed on a (301) HgCdTe surface. A comparison and analysis of these images allow to find the correlation between peculiarities of micromorphology in the defect area and its microstructure. Fig. 3 shows the scheme for the analysis of the V-shaped defect

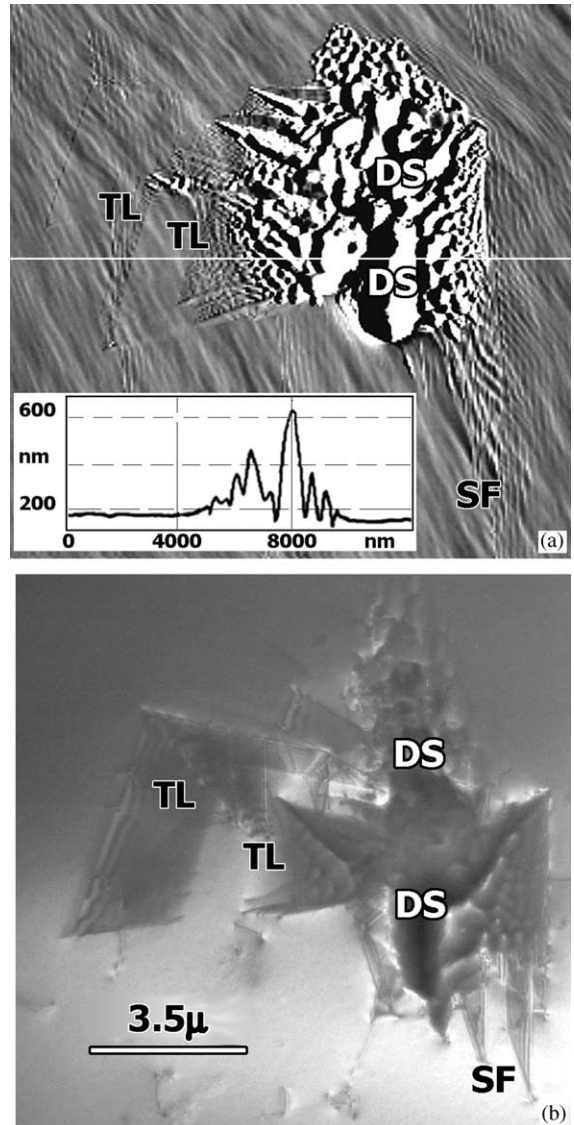


Fig. 2. Typical AFM image,  $12 \times 12 \mu\text{m}^2$  scan (a) and TEM image (b) of a V-shaped defect composed of TLs, SFs and DS on the surface of a (301) HgCdTe film. The inset in (a) shows the relief profile along the white line.

image. In this scheme, the pyramid formed by  $\{111\}$  planes inclined to the (301) surface (a) and the quadrangle being the trace of the intersection of this pyramid with the (301) surface (b) are represented. In Fig. 2 we see the typical elements of V-shaped defects: SFs, TLs, DS areas. The height profile along the white line in (a) is shown in

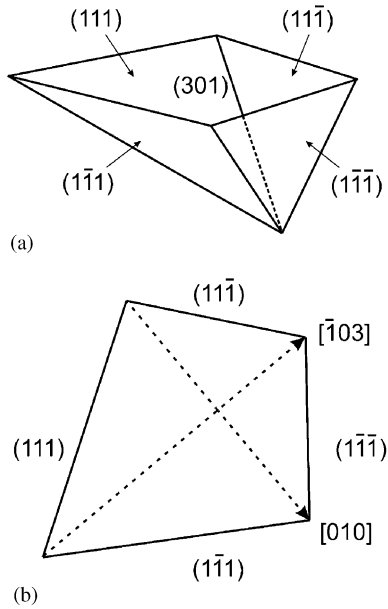


Fig. 3. The pyramid formed by  $\{111\}$  planes inclined to the  $(301)$  surface (a) and the trace of intersection of this pyramid with the  $(301)$  surface (b).

the inset. The height of DS area is over 500 nm. The SFs and TLs grow along  $\{111\}$  planes from the V-shaped defect center. When the V-shaped defect image is compared with the scheme shown in Fig. 3, it is evident that the defect is bounded to the right by the  $(1\bar{1}\bar{1})$  plane which is inclined at  $68.58^\circ$  to the  $(301)$  plane and to the left by the set of  $(111)$  planes which are inclined at  $43.09^\circ$  to the  $(301)$  plane. TEM investigation of cross-sections shows that essentially all SFs observed in  $(301)$  HgCdTe layers are located in  $(1\bar{1}\bar{1})$  planes, growing from the CdTe buffer layer. SFs which lie in  $(111)$  planes are observed only in the area of the V-shaped defect. The areas with disordered structure in the center part of the V-shaped defect present the most hazard to photo-diodes. Thus, the formation mechanism and microstructure of these areas were closely studied.

At low defect density (less than  $10^3 \text{ cm}^{-2}$ ) TEM investigation is difficult because of the small size of electron-transparent foil area and low defect density. To follow the consecutive stages of V-shaped defect formation by TEM, it is good to use the growth of HgCdTe layers under non-optimal

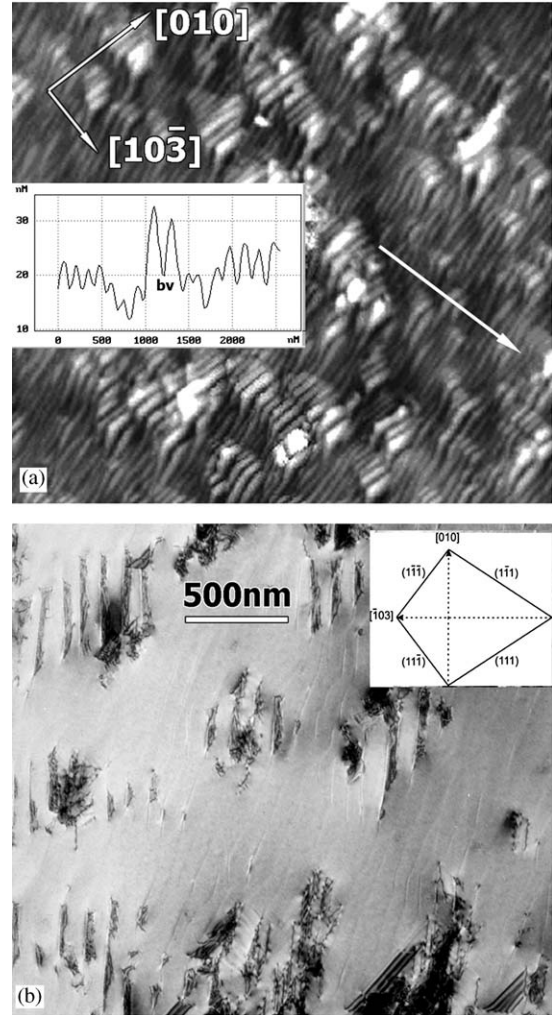


Fig. 4. AFM image,  $9 \times 9 \mu\text{m}^2$  scan (a) and TEM image (b) of the surface of  $(301)$  HgCdTe grown under non-optimal conditions.

conditions: elevated temperatures and reduced Hg vapor pressure. Under these conditions, continual V-shaped defect nucleation takes place and defect density may be as great as  $10^6 \text{ cm}^{-2}$ . In this case the possibilities for investigation of all defect formation stages, beginning from the initial ones, appear.

Fig. 4 shows images of the surface (a) and near-surface area (b) of a  $(301)$  HgCdTe layer grown under non-optimal conditions. One can see in Fig. 4a, that the peculiarity of this surface

micromorphology is the appearance of anisotropic relief as shown in Fig. 1a. The height profile along the white line in (a) is shown in an inset. There is a periodic alternation of valleys and ridges that are oriented approximately along the  $[0\ 1\ 0]$  direction. In some places the regular relief is perturbed: macrosteps change their directions and are oriented accurately along the  $[0\ 1\ 0]$  direction, and the height of macrosteps and distance between them increase, as can be seen in the inset in Fig. 4a. From TEM data it follows that in these places of relief perturbations an accumulation of dislocations is observed (Fig. 4b). The analysis of this TEM image allows one to reveal the consecutive stages of the V-shaped defects formation, beginning from the initial ones shown in Fig. 5a. The lines (line-shape areas) of disordered structure are seen well along the macrostep bends as dark lines with diffraction contrast. In Fig. 4a these lines of disordered structure are aligned between two ridges on the bottom of the valley (in the inset it is marked as “bv”). The microstructure along

these lines was observed with atomic resolution. The HREM image shows the presence of precipitates with the distance between atomic layers precisely the same as in elemental Te: 0.59 nm (see the inset in Fig. 5b). Fig. 5c shows the presence of misoriented fine HgCdTe grains. Since Te activity during HgCdTe growth by MBE is sufficient for elemental Te formation [ 9 ], it would appear reasonable to assume that under non-optimal conditions elemental Te can be accumulated along the growth front (along the macrosteps in the case of steady-state growth) and initiates the nucleation of misoriented HgCdTe grains and Te precipitates, in a size of 10 nm. In these places the macrosteps bend because its flow is pinning. As a result, short lengths of macrosteps can assume exact  $[0\ 1\ 0]$  direction, as follows from TEM data.

HgCdTe grains and Te precipitates can trigger the formation of dislocations, which are observed along the macrosteps bend, too (Fig. 4b). At this stage the formation of walls with HgCdTe grains, excess Te and dislocations begins. While HgCdTe

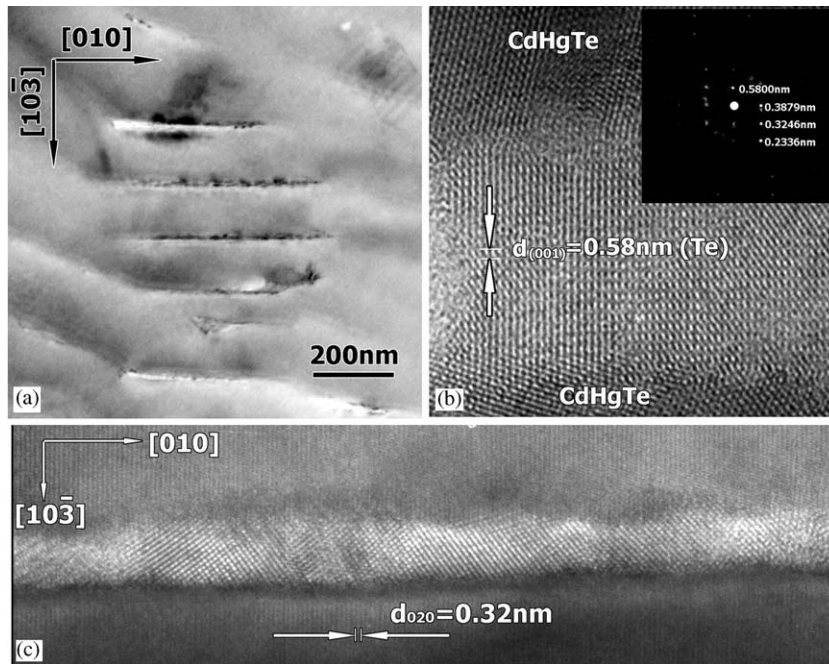


Fig. 5. Initial stage of V-shaped defect formation. (a) Bright-field TEM image of the disordered structure that is formed along  $[0\ 1\ 0]$  macrosteps,  $g = 040$ ; (b) HREM image and corresponding microdiffraction pattern of Te precipitates; (c) HREM image of misoriented fine HgCdTe grains that are formed along  $[0\ 1\ 0]$  macrosteps; the orientation of HgCdTe grains is close to  $(0\ 0\ 1)$ . The incident e-beam direction is  $[3\ 0\ 1]$  (a,c) and  $[1\ 1\ 0]$  (b).

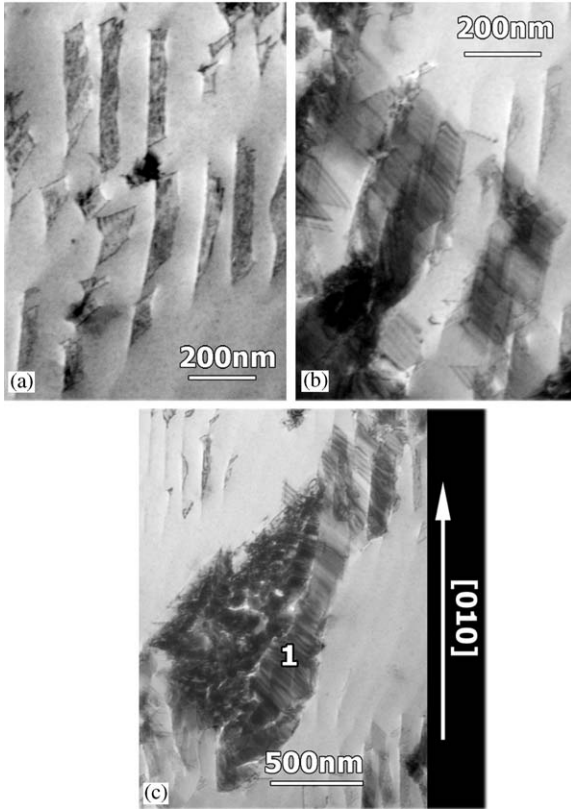


Fig. 6. Bright-field TEM-images of DS walls along macrosteps (a), SFs bounded by DS walls and partial dislocations located in DS walls (b), the column packed with SFs -1 and defect shaped around it (c). All images were obtained after  $18^\circ$  tilting of the specimen around the  $[010]$  axis toward the  $(100)$  pole,  $g = 022$ .

layer growth occurs, these walls with disordered structure extend along the growth direction. Hereafter, we shall use the term “DS walls” to mean “walls with disordered structure”. The TEM image of these DS walls is shown in Fig. 6. Stereophotography was used to locate these DS walls. The DS wall images shown in Fig. 5a were obtained under the imaging conditions close to the  $[301]$  zone axis (when the incident e-beam direction is perpendicular to the  $(301)$  surface). Under these conditions of observation, the width of the DS wall image is minimum. When the sample is tilted  $18^\circ$  about the  $[010]$  axis to the left (towards the  $(100)$  pole) and to the right (towards the  $(101)$  pole), the DS wall image becomes wider and appears to the right and to the left from the

$[010]$  direction, respectively. This indicates that the DS walls are normal to the  $(301)$  growth surface. The DS walls observed by TEM intersect the  $(301)$  growth surface in the  $[010]$  direction. From the analysis of a stereographic projection for the  $(301)$  plane, it follows that the DS walls are located in vertical  $(103)$  planes, which are perpendicular to the  $(301)$  plane and intersect it along the  $[010]$  direction. The formation of DS walls extended along the growth direction and containing HgCdTe grains, Te precipitates and dislocations may be considered the initial stage of V-shape defect formation.

While growing, under the action of strains the perfect dislocations located in the DS walls split up partial dislocations and SFs between them. One partial dislocation is in the original DS wall, but another one glides along the  $(1\bar{1}1)$  plane to the nearest DS wall and is located in it (Fig. 6b). It is evident from TEM image analysis that the straight partial dislocations bounding the SFs are oriented in the direction that projection on the  $(301)$  plane is coincident with the  $[010]$  direction (Fig. 6b). This is possible only when the partial dislocations are located in  $(103)$  planes which are normal to the  $(301)$  growth surface. Consequently, the vertical DS walls bound the gliding of partial dislocations and lateral SF growth. As a result, while growing, vertical columns packed with SFs (with  $(1\bar{1}1)$  twinning plane) extended along the growth direction and bounded by DS walls are formed. An example of this column is represented in Fig. 6c (mark 1). The relief perturbation near these columns can initiate Te-segregation, DS wall formation and nucleation of new SFs. This process can take an avalanche-type character under non-optimal growth conditions and result in the fast growth of defect area over the surface. As this takes place, V-shaped defect sizes can be as large as  $20\text{--}50\ \mu\text{m}$  or more in diameter for films of  $10\ \mu\text{m}$  thickness. In addition to twinning within the columns, the nucleation of new extended SFs in other  $\{111\}$  planes inclined to the surface takes place too. And the defect shown in Fig. 6c is shaped. It is seen that this defect morphology is like the morphology of the V-shaped defect segment shown in Fig. 2b. The area of disordered structure, marked as DS in Fig. 2, represents the

column of SFs (or microtwins) like the column shown in Fig. 6c. This is supported by the presence of twin reflections on the microdiffraction pattern obtained from the DS areas. In Figs. 2 and 6c it is well seen that extended SFs and TLs grow from the DS area (which is in the defect center) along inclined  $(111)$  and  $(1\bar{1}\bar{1})$  planes, increasing the lateral size of the V-shaped defect as film growth occurs.

From the above results, it follows that Te segregation on the relief perturbations under non-optimal growth conditions leads to the formation of DS walls, columns packed with SFs between them and eventually V-shaped defect formation. The maintenance of growth conditions within the optimal growth “window” allows one to prevent the V-shaped defect formation in the steady-state stages of HgCdTe growth.

In the initial stages of HgCdTe layer growth, the situation is complicated by the fact that the optimal growth conditions are not attained yet, whereas the relief perturbations on the substrate surface are present. In the experiments carried out, the CdTe buffer layer plays the role of a substrate. Our investigation of CdTe buffer layers by TEM and AFM revealed that the surface irregularities with heights more than 10–20 nm are the emergence of threading defects. The detailed analysis of the defect structure of CdTe buffer layers is not discussed in this paper. However, we point out that the steps that are obtained from intersection of inclined microtwins with the growth surface and hillocks are more common surface irregularities in our CdTe buffer layers. According to TEM and AFM investigations, we can say that the hillocks on CdTe surface are caused by the particles built into the CdTe layer. The origin of these particles is either substrate-related [13] or growth-related. The SFs and microtwins originated at the substrate-epilayer interface. We have established that just these surface irregularities made Te segregation much easier, and represent the places of origin of V-shaped defects at the initial stages of HgCdTe growth. As an example of V-shaped defects which originated at the CdTe buffer layer/HgCdTe film interface, we represent two more typical defect images observed in  $(301)$  HgCdTe films in Figs. 2 and 7. These V-shaped defects have a common

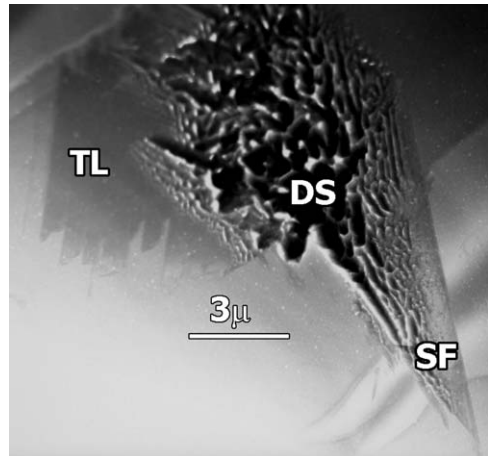


Fig. 7. TEM image of a V-shaped defect in HgCdTe film which was formed around the hillock on the CdTe surface.

nature, but different shaped DS areas: extended (Fig. 2) and rounded (Fig. 7). The DS area of the defect shown in Fig. 2 is extended along the steps on the CdTe surface formed by the set of microtwins along  $(1\bar{1}\bar{1})$  planes. The DS area of the defect shown in Fig. 7 was formed around the hillock on CdTe surface. The height of the hillock in the center of the DS area can exceed 1000 nm. Thus, we can say that two typical CdTe surface irregularities result in two typical V-shaped defect images.

TEM investigation of  $(112)$  HgCdTe layers has suggested that, as well as in  $(301)$  HgCdTe layers, the V-shaped defect formation mechanism is based on the formation of DS walls extended along the growth direction with columns of microtwins between them (Fig. 8). The plan-view image (Fig. 8c) shows the surface of the film grown under non-optimal conditions: there is the anisotropic relief with macrosteps extended along the  $[11\bar{1}]$  direction and top-view of the V-shaped defect. The cross-section images (Fig. 8a, b) show the columns packed with microtwins and separated by DS walls.

#### 4. Conclusion

The microstructure of V-shaped defects in  $(301)$  and  $(112)$  HgCdTe layers grown by MBE was

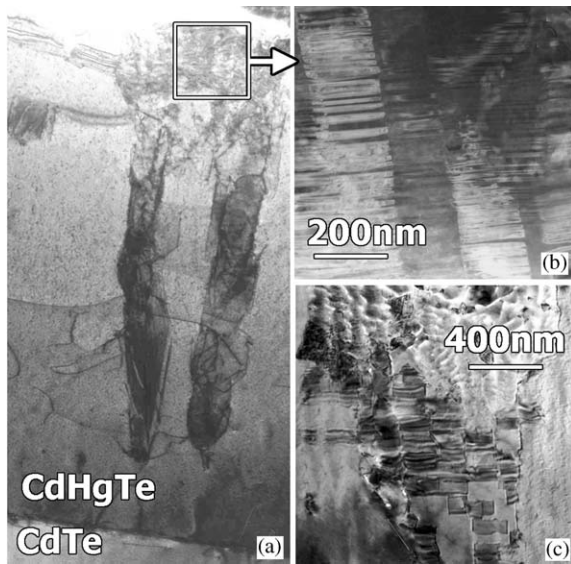


Fig. 8.  $(1\ 1\ \bar{1})$  cross-section (a, b) and  $(1\ 1\ 2)$  plan view (c) TEM images of a V-shaped defect in  $(1\ 1\ 2)$  HgCdTe; (b) the columns of microtwins observed inside the area marked by the white square in (a).

studied in detail on consecutive stages of its formation by TEM, HREM and AFM. The formation mechanism of V-shaped defects was presented. It was shown that the nucleation of V-shaped defects occurs on the relief perturbations. The nucleation and the growth of V-shaped defects are stimulated by non-optimal growth conditions: high substrate temperature and low Hg-vapor pressure. The formation of the V-shaped defect begins from the capture of excess Te along the growth front at steady-state stages of HgCdTe growth and along the irregularities on the surface of CdTe buffer layer at the initial stages. The captured Te initiates the nucleation of misoriented HgCdTe grains, new Te precipitates and dislocations in the vertical walls that are formed along the growth front under non-optimal growth conditions. It was established that the formation of these walls with disordered structure (DS walls) extended along the growth direction is the initial stage of V-shaped defect formation. Under the effect of strains, the splitting of perfect dislocations into partial ones with SF between them takes place. DS walls bound the gliding of partial dislocations and lateral SF growth. While grow-

ing, vertical columns packed with SFs and bounded by DS walls are formed. These columns represent the basic part of the V-shaped defect: DS area. Due to continual Te nucleation and twinning, polycrystalline growth in the DS area can occur. The extended SFs and TLs grow from the DS areas along  $\{1\ 1\ 1\}$  planes. With film thickness growth, the size of DS areas increases as well as the sizes of extended SFs and TLs. As a result, the lateral size of the V-shaped defect increases with HgCdTe film thickness.

### Acknowledgments

The authors would like to thank N.N. Michailov and M.V. Yakushev for providing HgCdTe epilayers.

### References

- [1] D. Chandra, F. Aqariden, J. Frazier, S. Gutzler, T. Orent, H.D. Shih, *J. Electron. Mater.* 29 (2000) 887.
- [2] D. Chandra, H.D. Shih, F. Aqariden, R. Dat, S. Gutzler, M.J. Bevan, T. Orent, *J. Electron. Mater.* 27 (1998) 640.
- [3] L. He, Y. Wu, L. Chen, S.L. Wang, M.F. Yu, Y.M. Qiao, J.R. Yang, Y.J. Li, R.J. Ding, Q.Y. Zhang, *J. Crystal Growth* 227 (2001) 677.
- [4] M. Zandian, E. Goo, *J. Electron. Mater.* 30 (2001) 623.
- [5] E.C. Piquette, M. Zandian, D.D. Edwall, J.M. Arias, *J. Electron. Mater.* 30 (2001) 637.
- [6] T. Aoki, Y. Chang, G. Badano, J. Zhao, C. Grein, S. Sivananthan, D.J. Smith, *J. Electron. Mater.* 32 (2003) 703.
- [7] Y. Chang, G. Badano, J. Zhao, C.H. Grein, S. Sivananthan, T. Aoki, D.J. Smith, *Appl. Phys. Lett.* 83 (2003) 4785.
- [8] T. Aoki, David J. Smith, Y. Chang, J. Zhao, G. Badano, C. Grein, S. Sivananthan, *Appl. Phys. Lett.* 82 (2003) 2275.
- [9] I.V. Sabinina, A.K. Gutakovsky, Yu.G. Sidorov, S.A. Dvoretzky, V.D. Kuzmin, *J. Crystal Growth* 117 (1992) 238.
- [10] V.S. Varavin, S.A. Dvoretzky, V.I. Liberman, N.N. Mikhailov, Yu.G. Sidorov, *Thin Solid Films* 267 (1995) 121.
- [11] Yu.G. Sidorov, M.V. Yakushev, D.N. Pridachin, V.S. Varavin, L.D. Burdina, *Thin Solid Films* 367 (2000) 203.
- [12] I.V. Sabinina, A.K. Gutakovsky, *Ultramicroscopy* 45 (1992) 411.
- [13] M. Zandian, J.M. Arias, J. Bajaj, J.G. Pasko, L.O. Bubulac, R.E. DeWames, *J. Electron. Mater.* 24 (1995) 1207.